

Quantum reactive scattering in three dimensions using adiabatically adjusting principal axis hyperspherical coordinates: Periodic distributed approximating functional method for surface functions

Keming Zhang and Gregory A. Parker^{a)}

Department of Physics and Astronomy, University of Oklahoma, Norman, Oklahoma 73019

Donald J. Kouri

Department of Chemistry and Department of Physics, University of Houston, Houston, Texas 77204-5641

David K. Hoffman

Department of Chemistry and Ames Laboratory, Iowa State University, Ames, Iowa 50011

Srinivasan S. Iyengar

The Henry Eyring Center for Theoretical Chemistry and Department of Chemistry, The University of Utah, Salt Lake City, Utah 84112

(Received 15 July 2002; accepted 15 October 2002)

Periodic distributed approximating functionals are proposed and used to obtain a coordinate representation for the adiabatically adjusting principal axis hyperspherical coordinate kinetic energy operator. The approach is tested and accurate results for adiabatic surface functions for the reaction $F + H_2 \rightarrow HF + H$ are calculated and compared to those of some existing methods. © 2003 American Institute of Physics. [DOI: 10.1063/1.1526835]

I. INTRODUCTION

As is well known,^{1–11} there has been tremendous progress in recent years in accurate quantum calculations on exchange (rearrangement) reactions of the form



and these now include cases in which four atoms¹² are present (i.e., where C is replaced by CD in the above reactions) as well as the above three-atom reaction. Many of these methods use hyperspherical coordinates and are efficient; however, the accurate solution of the quantum Schrödinger equation continues to be computationally intensive. Hence, there is a real need to make the codes more efficient and accurate, especially if one is interested in collisions involving multiple electronic states or collision-induced dissociation.

In the hyperspherical coordinate formulation of triatomic reactive scattering, composed of a hyper-radius and five angular coordinates, the total wave function is expanded in a complete set of products of Wigner D functions for the three Euler angles “external angles” describing the spatial orientation of the three-particle plane, times basis functions or surface functions which depend on the remaining two “internal” hyperspherical angles. The dependence of the expansion coefficients on the hyper-radius, which is a measure of the size of the three-particle system, is then determined by propagating the solution of a set of coupled-channel (CC) differential equations from a small hyper-radius, where the solutions must be regular because the atoms coalesce, to a large hyper-radius where the wave function is projected onto

the arrangement channels and analytic boundary conditions are used to determine the scattering matrix. In the methods using hyper-spherical coordinates that treat all particles symmetrically,^{8–10,13–17} one numerically obtains “surface functions,” the basis functions of the two hyper-angles, by numerically solving a two-dimensional (2D) Schrödinger equation. This Schrödinger equation, which is discussed in more detail later in this paper (see Sec. III), depends parametrically on the hyper-radius and must be solved at many values of the hyper-radius. In addition, a large number of surface functions must be obtained at each hyper-radius, and hence efficient computational procedures for numerically solving this 2D Schrödinger equation are essential.

The first accurate fully three-dimensional (3D) reactive scattering calculations employing hyper-spherical coordinates used finite element methods (FEMs)^{9–11,14,17–19} to solve for the surface functions. Although these FEMs give fairly accurate results, they are inefficient and not robust. Another commonly used method involves the use of the discrete variable representation (DVR),^{14,15,20–22} which is most efficient at small hyper-radii where the surface functions are delocalized. At larger values of the hyper-radius, where the surface functions are highly localized, the DVR points cover the whole space, making the method much less efficient. In a few cases the DVR is even more expensive than the FEM because of the need for many grid points in a small, localized region. Other methods such as the finite basis representation (FBR)^{8,13,16} of Launay and LeDourneuf, and the method of Wolniewicz and Hinze²³ are also efficient only at large hyper-radii. The analytic basis method (ABM) uses primitive rovibrational basis functions centered in the arrangement channels, and provides a very compact representation and thus is quite efficient at large hyper-radii, but is inefficient

^{a)}Electronic mail: parker@phyast.nhn.ou.edu

and the basis is overcomplete at small hyper-radii.²⁴

In this paper, we present the periodic distributed approximating functional (PDAF) method, an approach that is efficient at both small and large values of the hyper-radius. The PDAF method is similar to the symmetry-adapted-Hermite distributed approximating functional (SA-HDAF) approach of Iyengar *et al.*,²⁵ but differs importantly by involving only real symmetric matrices. In addition, in the present approach only the surface functions are obtained, while in the SA-HDAF approach²⁵ the full 3D wave function was obtained directly, by using an iterative procedure. The symmetry adaptation of the PDAF is carried out here in a similar, but simpler, fashion than in Ref. 25. Here we employ the distributed approximating functional (DAF) concept, but the PDAF differs from all previous DAFs. However, like other DAFs it is both accurate and efficient as a computational tool. A more detailed exposition of the connections between the PDAF and the Christoffel–Darbeaux formula for DAFs based on orthogonal polynomials will follow.²⁶ The sequential diagonalization-truncation technique^{27,28} is employed to project the large-size Hamiltonian matrix into a smaller matrix using a projection matrix which is obtained by solving a one-dimensional eigensystem, thus significantly reducing the memory requirements and the computation time.

This paper is organized as follows: In Sec. II we introduce the PDAFs and derive their formulas. In Sec. III the rovibrational triatomic Hamiltonian in the adiabatically adjusting principal axis hyperspherical (APH) coordinates system is presented and the symmetrization and reductions of the Hamiltonian are illustrated. The PDAF approach is then tested in Sec. IV. Surface functions for the FH₂ scattering system are computed, and the eigenenergies and the matrix elements are calculated and compared to those of existing methods (FEM, ABM, and DVR) in Sec. V. In Sec. VI we present our conclusions.

II. PERIODIC DISTRIBUTED APPROXIMATING FUNCTIONAL (PDAF)

Consider any continuous periodic function, $f_p(x)$, for convenience scaled to have period 2π . From the definition of the Dirac delta function, we know that

$$\begin{aligned} f_p(x) &= \int_{-\infty}^{\infty} \delta(x-x') f_p(x') dx' \\ &= \sum_{m=-\infty}^{\infty} \int_0^{2\pi} \delta(x-x'-2m\pi) f_p(x'+2m\pi) dx', \end{aligned} \quad (2)$$

where we have expressed the integration range as an infinite sum of segments of length 2π . Interchanging the integral and sum, and using the periodicity of $f_p(x)$, we have

$$\begin{aligned} f_p(x) &= \int_0^{2\pi} \sum_{m=-\infty}^{\infty} \delta(x-x'-2m\pi) f_p(x') dx' \\ &= \int_0^{2\pi} \delta_p(x-x') f_p(x') dx', \end{aligned} \quad (3)$$

where

$$\delta_p(x-x') = \sum_{m=-\infty}^{\infty} \delta(x-x'-2m\pi), \quad (4)$$

is the periodic delta function. Since $\delta(x)$ is an even function, it's easy to see that $\delta_p(x)$ is even and is also periodic with a period of 2π . The k th derivative of $f_p(x)$ is then given by

$$f_p^{(k)}(x) = \int_0^{2\pi} \delta_p^{(k)}(x-x') f_p(x') dx'. \quad (5)$$

Expanding $\delta_p(x-x')$ in a Fourier series, we obtain

$$\delta_p(x-x') = \frac{1}{\pi} \left(\frac{1}{2} + \sum_{n=1}^{\infty} \cos n(x-x') \right), \quad (6)$$

for the periodic delta function.

We define the partial sum of the periodic delta function to be the continuous periodic distributed approximating functional (PDAF)

$$\begin{aligned} \delta_{p,M}(x-x') &\equiv \frac{1}{\pi} \left[\frac{1}{2} + \sum_{n=1}^M \cos n(x-x') \right] \\ &= \frac{1}{2\pi} \left\{ \frac{\cos[(M-1)(x-x')] - \cos[M(x-x')]}{1 - \cos(x-x')} \right\}, \end{aligned} \quad (7)$$

which is the basic result used in this work. The last expression is obtained by noting that $\delta_{p,M}(x-x')$ is the real part of a sum of exponentials which can be written as a geometric sum and thus done analytically. By definition, as M increases, the PDAF approaches the periodic delta function, i.e., $\delta_p(x-x') = \lim_{M \rightarrow \infty} \delta_{p,M}(x-x')$.

One may obtain the fully discretized PDAF by approximating the integral over x' in Eq. (5) using a trapezoidal quadrature

$$f_{p,M}^{(k)}(x) = \sum_{j=1}^N \delta_{p,M}^{(k)}(x-x_j) f_p(x_j) \Delta x, \quad (8)$$

where N is the number of grid points, $\Delta x = 2\pi/N$, and $x_j = (j - \frac{1}{2})\Delta x$. This choice of quadrature points is particularly useful if we are solving differential equations with singular points at the two ends ($x=0$ and $x=2\pi$). As the grid points are fixed, $\delta_{p,M}^{(k)}(x)$ acts like the discretized k th derivative operator. One can also discretize x using the same grid points as used in the numerical quadrature. If we treat the discretized $f_{p,M}(x)$ and its derivatives as a column vector, e.g., $[f_j = f(x_j)]$, we have

$$f_i^{(k)} = \sum_{j=1}^N D_{ij}^{(k)} f_j, \quad (9)$$

where

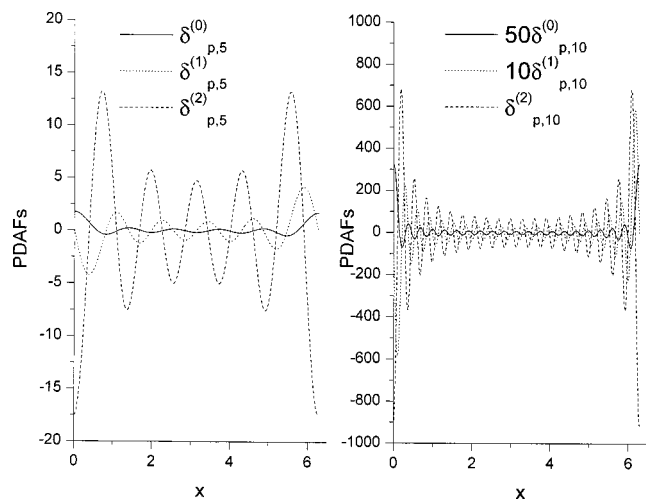


FIG. 1. $\delta_{p,M}^{(k)}(x)$ for different M , where the number of grid points ($N=20$) is used in both panels. In the left panel $M=5$ and in the right panel $M=N/2=10$. Note $\delta_{p,M}^{(0)}$ and $\delta_{p,M}^{(2)}$ are symmetric about $x=0$, while $\delta_{p,M}^{(1)}$ is antisymmetric. Increasing M makes the PDAFs sharply peaked and a better representation of the respective delta function and its derivatives.

$$D_{ij}^{(k)} = \delta_{p,M}^{(k)}(x_i - x_j) \Delta x$$

$$= \begin{cases} (-1)^{(k+1)/2} \frac{\Delta x}{\pi} \sum_{n=1}^M n^k \sin n[(x_i - x_j)] x & k \text{ odd} \\ \frac{\Delta x}{2\pi} \delta_{0,k} + (-1)^{k/2} \frac{1}{\pi} \sum_{n=1}^M n^k \cos n[(x_i - x_j)] & k \text{ even} \end{cases} \quad (10)$$

is the k th derivative operator in matrix form. The differential operators, $D^{(k)}$, are periodic Toeplitz matrices which depend on only one parameter, M . As M increases, the PDAF gives an increasingly accurate representation of the Dirac delta function. However, it is for small M that the integrand of Eq. (5) is smoothest and the trapezoidal rule is most accurate. Hence, we seek an optimal compromise value of M . Since the integrand involves a Fourier function, the theory of Gaussian quadrature suggests a relation of $M=N/2$. Through numerical experimentation (see Sec. IV) we verify that this value gives the most accurate results. In this paper, we will use $D^{(0)}$, $D^{(1)}$, and $D^{(2)}$; consequently, we need $\delta_{p,M}^{(0)}$, $\delta_{p,M}^{(1)}$, and $\delta_{p,M}^{(2)}$. They can be obtained simply by differentiating Eq. (7).

We see that $\delta_{p,M}^{(k)}(x)$ are even(odd) periodic functions when k is even(odd). The functions, $\delta_{p,M}^{(0)}(x)$, $\delta_{p,M}^{(1)}(x)$, and $\delta_{p,M}^{(2)}(x)$, which are the ones used in this paper, are shown in Fig. 1. In both panels of Fig. 1 $N=20$, in the left panel $M=5$, and in the right panel $M=N/2=10$. One can readily see the symmetry of each PDAF. Comparing the left and right panels in Fig. 1, we see that increasing M makes the PDAFs in the right panel sharply peaked and a better approximate representation of the periodic Dirac delta function and its derivatives.

The equations obtained in this section for the PDAF, namely Eq. (7) and Eq. (10) may be compared with those obtained using the SA-HDAF²⁵ for functions with periodic symmetry, namely Eq. (5) and associated expressions in Ref.

25. It is clear that both representations are Toeplitz; however, the expression in Ref. 25 has the additional characteristic of being banded, which is not the case in the present formulation. However, as we will see later in this paper, this does not present any problems in the current implementation and in fact helps to enhance the accuracy of the procedure introduced here.

III. SYMMETRIZATION AND REDUCTIONS OF THE TRIATOMIC HAMILTONIAN IN APH COORDINATES

A. APH Hamiltonian

The detailed reactive scattering theory formulated in adiabatically adjusting principle axis hyper-spherical (APH) coordinates has been presented previously,⁹ and we repeat only the essentials here. In this approach, one needs sector adiabatic basis functions $\Phi_{\tau\Lambda}^p$ of the APH hyper-angles, and in this work we choose surface functions, $\Phi_{\tau\Lambda}^p$, defined by the equation

$$H\Phi_{\tau\Lambda}^p(\theta, \chi; \rho_\xi) = \mathcal{E}_{\tau\Lambda}^p(\rho_\xi)\Phi_{\tau\Lambda}^p(\theta, \chi; \rho_\xi), \quad (11)$$

where H is a portion of the full Hamiltonian omitting parts of the orbital angular momentum. Thus, we take

$$H = -\frac{\hbar^2}{2\mu\rho_\xi^2} \left[\frac{4}{\sin 2\theta} \frac{\partial}{\partial \theta} \sin 2\theta \frac{\partial}{\partial \theta} + \frac{1}{\sin^2 \theta} \frac{\partial^2}{\partial \chi^2} \right] + \frac{15\hbar^2}{8\mu\rho_\xi^2} + C\hbar^2\Lambda^2 + V(\rho_\xi, \theta, \chi). \quad (12)$$

The first term in the Hamiltonian H is the ‘‘hyper-spherical’’ part of the kinetic energy operator, and $C=1/[\mu\rho_\xi^2(1-\sin\theta)]$ is part of the centrifugal potential. The potential energy V used here is the complete potential energy surface (PES) of Brown *et al.*,²⁹ and the $\mathcal{E}_{\tau\Lambda}^p(\rho_\xi)$ are the eigenenergies of H at the hyper-radius ρ_ξ . The variable θ is the APH bending angle; its range is $0 \leq \theta \leq \pi/2$, with $\pi/2$ describing linear configurations and 0 describing triangular symmetric top configurations. The variable χ is the APH kinematic angle measured from the ‘‘incident’’ arrangement channel; it measures motion between arrangement channels, and its range is $-\pi \leq \chi \leq \pi$. The angles θ and χ cover the upper half of the surface of an internal coordinate sphere which we loosely call the ‘‘hypersphere.’’ (More precisely, the surface of the hyper-sphere is the 5D space covered by θ , χ , and the three Euler angles which describe the orientation of the principal axes in space. In fact, the hyper-sphere may be decomposed into two commuting subgroups, $O(2)$ and $O(3)$, and this aspect has been exploited in computing surface functions with fixed total angular momentum.⁹) As one can see from Eq. (11) the surface functions $\Phi_{\tau\Lambda}^p$ and eigenenergies $\mathcal{E}_{\tau\Lambda}^p$ depend parametrically on the hyper-radius ρ_ξ . They are needed at a set of ρ values $\{\rho_\xi\}$, $\xi=1, 2, \dots, n_\rho$, and are used as adiabatic basis functions for expanding the full wave function in each sector where $(\rho_\xi + \rho_{\xi-1})/2 \leq \rho \leq (\rho_{\xi+1} + \rho_\xi)/2$ for sector ξ . As shown elsewhere,⁹ this diabatic-by-sector (or sector-adiabatic) expansion of the wave function gives rise to a set of coupled second-order differential equations. The three quantum numbers (Λ, p, τ) labeling $\mathcal{E}_{\tau\Lambda}^p$ and $\Phi_{\tau\Lambda}^p$ are: Λ , the component of the total angular momentum

along the APH body-frame (BF) z axis (the axis of least inertia of the three-body system), p is the parity quantum number with $p=0$ or 1 , the parity of $\Phi_{\tau,\Lambda}^p$ under the parity transformation $\chi \rightarrow \chi \pm \pi$ is $(-1)^p$, and $\tau=1,2,\dots,n_\Phi$, which indexes the solutions in order of increasing energy. These coupled-channel (CC) equations must be numerically integrated from a small value of the hyper-radius ρ where the full wave function is zero to a large value of the hyper-radius where asymptotic boundary conditions are applied. The quantity μ is the three-body reduced mass of the system arising from using mass-scaled coordinates.

Equation Eq. (12) differs from Eq. (164) of Ref. 9 slightly because it omits a rotational term of the form $\frac{1}{2}(A+B)\hbar^2[J(J+1)-\Lambda^2]$ as mentioned above. As pointed out by Launay and LeDourneuf,⁸ this gives surface functions $\Phi_{\tau,\Lambda}^p$ which are independent of the total angular momentum J , so many fewer surface functions must be calculated. The omitted term is easily included in the CC equations along with the remaining Coriolis and asymmetric top terms. This surface function basis is expected to produce rapid convergence of the CC expansion to the exact solution provided triangular symmetric top ($\theta=0$) configurations are unimportant, which is the case for many reactions.

The full wave function must be continuous and regular everywhere. This requires that $\Phi_{\tau,\Lambda}^p$ must also be a continuous function of χ at $-\pi$ and π and regular everywhere. For systems with two or three identical atoms, the surface functions have other symmetries in addition to the parity, p , already defined and these symmetries will be exploited. The surface functions are real and normalized according to

$$\int_{-\pi}^{\pi} d\chi \int_0^{\pi/2} \Phi_{\tau,\Lambda}^{p'}(\theta,\chi;\rho_\xi) \Phi_{\tau,\Lambda}^p(\theta,\chi;\rho_\xi) \sin 2\theta d\theta = \delta_{\tau',\tau} \delta_{p',p}. \quad (13)$$

The surface function Hamiltonian, Eq. (12) is

$$H = \frac{\hbar^2}{2\mu\rho_\xi^2} \left[H_\theta + \frac{1}{\sin^2 \theta} H_\chi \right] + H_V, \quad (14)$$

where H_θ , H_χ , and H_V are obviously defined by comparing Eq. (12) with Eq. (14). The discretized Hamiltonian is a matrix operator. In the rest of this paper, we use the term Hamiltonian to refer to this matrix.

B. Symmetrization of APH Hamiltonian

The Hamiltonian H in Eq. (14) is real but it is not symmetric, because H_θ is not symmetric. Therefore, if we use this form, we have to solve a nonsymmetric matrix eigensystem requiring a large amount of memory and CPU time. It is therefore critical in the computation of APH surface functions to symmetrize H . The matrix H_θ is the nonsymmetric part of H , and it is not periodic. We first extend H_θ to a periodic form and symmetrize it. Then, the result is extended to symmetrize H .

Although H_θ is defined initially on $0 \leq \theta \leq \pi/2$, we note that it is invariant under the transformation $\theta \rightarrow \pi - \theta$, and hence we can expand the domain of $\psi(\theta)$, the eigenfunction of H_θ , to the full real space by defining, $\psi(\theta) = \psi(\pi - \theta)$,

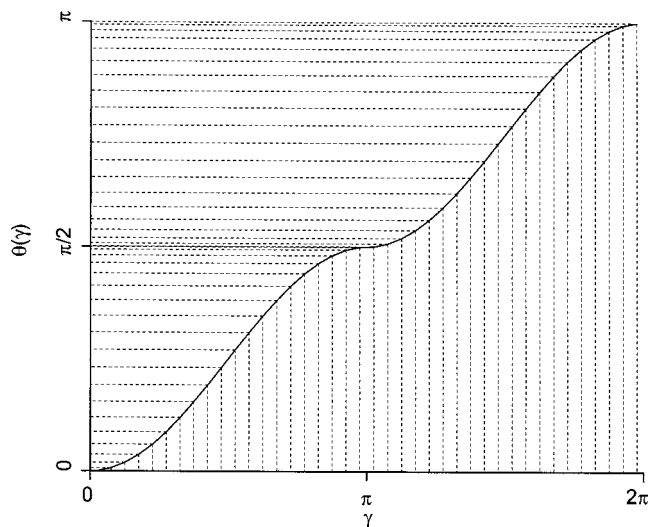


FIG. 2. Grid mapping function $\theta(\gamma)$. The uniform grid in θ corresponds to the nonuniform grid for θ which is dense near the singularities ($\theta=k\pi/2$) and sparse otherwise.

$[\pi/2 \leq \theta \leq \pi]$ $\psi(\theta+k\pi) = \psi(\theta)$, $[0 \leq \theta \leq \pi]$ for any integer value k . Now, $\psi(\theta)$ is a periodic function with a periodicity of π . Note that $H_\theta(\theta) = H(\pi - \theta)$, and $H_\theta(\theta+k\pi) = H(\theta)$. One can see that the extended $\psi(\theta)$ satisfies $H_\theta\psi(\theta) = \lambda\psi(\theta)$ for any θ , i.e., the domain of H_θ is also extended to the full real space although it keeps its original form.

We comment that similar expressions for H_θ were obtained in Ref. 25 by using a symmetry adaptation procedure, wherein H_θ was projected on the right side onto a function belonging to the A_1 irreducible representation of the point group C_{2v} , and on the left side onto a function belonging to the A_2 irreducible representation of the point group C_{2v} . The choice of the A_1 irreducible representation conforms with the θ periodic symmetry requirements. The A_2 irreducible representation was chosen due to the fact that the first derivative of an A_1 function is an A_2 function in C_{2v} . The resultant representation for H_θ in Ref. 25 is, however, not symmetric.

To obtain a symmetric representation for H_θ , we transform it in two steps. First, we introduce a continuous mapping function, $\theta(\gamma) = \pi/4 [1 - \cos(\gamma + 2k\pi)] - k\pi$, $k=0, \pm 1, \pm 2, \dots$. We note that the first derivative of this mapping is also continuous, but its second derivative is discontinuous at $\theta = k\pi/2$. This problem is handled by the mapping function itself: if we use a uniform grid for γ , it is equivalent to using a nonuniform grid for θ which is dense near the singularities ($\theta = k\pi/2$) and sparse otherwise, as shown in Fig. 2. Since more grid points are used in the $\theta = k\pi/2$ region, high accuracy can be obtained despite the discontinuity.

Substituting θ with γ in H_θ , we obtain

$$H_\theta(\gamma) = -\frac{64}{\pi^2} \frac{1}{\sin 2\theta(\gamma) \sin \gamma} \frac{\partial \sin 2\theta(\gamma)}{\partial \gamma} \frac{\partial}{\sin \gamma} \frac{\partial}{\partial \gamma}. \quad (15)$$

$H_\theta(\gamma)$ is very similar to $H_\theta(\theta)$ except that it has a periodicity of 2π .

Applying $T^\dagger = T$ to $H_\theta\psi(\theta) = \lambda\psi(\theta)$ and inserting the identity $T^{-1}T$ between H_θ and $\psi(\theta)$, we obtain

$$H_\gamma T\psi(\theta) = \lambda T\psi(\theta), \quad (16)$$

where

$$H_\gamma = T^\dagger H_\theta(\gamma) T^{-1} = -\frac{64}{\pi^2} \frac{1}{\sqrt{\sin 2\theta(\gamma)\sin\gamma}} \times \frac{\partial}{\partial\gamma} \frac{\sin 2\theta(\gamma)}{\sin\gamma} \frac{\partial}{\partial\gamma} \frac{1}{\sqrt{\sin 2\theta(\gamma)\sin\gamma}} \quad (17)$$

is a symmetric Hamiltonian. Note that the singularities in T^{-1} are avoided by our choice of quadrature (see Sec. II).

The eigenfunction of H_γ is $\tilde{\psi}(\gamma) = T(\gamma)\psi(\theta(\gamma))$, which is always zero at $\gamma=0, \pi$, or 2π . It is not hard to see that extending $\psi(\theta)$ from $0 \leq \theta \leq \pi/2$ to $0 \leq \theta \leq \pi$ introduces undesired degenerate eigenvalues. If we reduce matrix H_γ from $0 \leq \theta \leq 2\pi$ to range $0 \leq \theta \leq \pi$ using the symmetry of ψ , we can eliminate those undesired degenerate eigenvalues. We use a grid similar to the one used for PDAF; $\gamma_j = (j - \frac{1}{2})\Delta\gamma$, with $1 \leq j \leq 2N_\gamma$ where $2N_\gamma$ is the number of grid points, and $\Delta\gamma = \pi/N_\gamma$ is the distance between two consecutive grid points. For simplicity, we use a subscript j to denote a term evaluated at γ_j , and we also define the following terms, $t_j = 1/\sqrt{\sin 2\theta(\gamma_j)\sin\gamma_j}$ and $s_j = \sin 2\theta(\gamma_j)/\sin\gamma_j$. Applying the derivative operator $D^{(1)}$ in Eq. (10) (substituting x with γ), the eigenequation Eq. (16) can be written as

$$\lambda \tilde{\psi}_i = \sum_{j=1}^N \sum_{k=1}^{2N} -\frac{64}{\pi^2} t_i D_{ik}^{(1)} s_k (D_{kj}^{(1)} + D_{k, 2N-j+1}^{(1)}) t_j \tilde{\psi}_j = \sum_{j=1}^N H_{\gamma_{ij}}^r \tilde{\psi}_j, \quad (18)$$

where

$$H_{\gamma_{ij}}^r = \sum_{k=1}^{2N} -\frac{64}{\pi^2} t_i D_{ik}^{(1)} s_k (D_{kj}^{(1)} + D_{k, 2N-j+1}^{(1)}) t_j. \quad (19)$$

In the above derivation, $\tilde{\psi}_j = \tilde{\psi}_{2N-j+1}$, $t_j = t_{2N-j+1}$, $s_j = s_{2N-j+1}$, and the periodicity of $D^{(1)}$ is employed. One should note that in Eq. (18) $1 \leq i \leq N_\gamma$ and $1 \leq j \leq N_\gamma$, which means $0 \leq \gamma \leq \pi$, so H_γ^r is reduced to the original domain. H_γ^r is the desired symmetric matrix form for H_θ . It is, however, interesting to note that the bracketed quantity $(D_{kj}^{(1)} + D_{k, 2N-j+1}^{(1)})$ in Eq. (19) is not an antisymmetric matrix, in contrast to Ref. 25. The full H_γ^r presented in Eq. (19) is symmetric by construction.

Similarly, we can transform and discretize H to obtain its symmetric form. Using Eq. (14), the Schrödinger equation Eq. (11) reads

$$\left\{ \frac{\hbar^2}{2\mu\rho_\xi^2} \left[H_\theta + \frac{1}{\sin^2\theta} H_\chi \right] + H_V \right\} \Phi_{\tau\Lambda}^p(\theta, \chi; \rho_\xi) = \mathcal{E}_{\tau\Lambda}^p(\rho_\xi) \Phi_{\tau\Lambda}^p(\theta, \chi; \rho_\xi). \quad (20)$$

We multiply by T^\dagger from the left on both sides of the above equation, and insert the identity $T^{-1}T$, to obtain

$$H^s \bar{\Phi}_{\tau\Lambda}^p(\gamma, \chi; \rho_\xi) = \mathcal{E}_{\tau\Lambda}^p(\rho_\xi) \bar{\Phi}_{\tau\Lambda}^p(\gamma, \chi; \rho_\xi), \quad (21)$$

where

$$H^s = \frac{\hbar^2}{2\mu\rho_\xi^2} \left[H_\gamma^r + \frac{1}{\sin^2\theta} H_\chi \right] + H_V \quad (22)$$

and $\bar{\Phi}_{\tau\Lambda}^p(\gamma, \chi; \rho_\xi) = T \Phi_{\tau\Lambda}^p(\theta, \chi; \rho_\xi)$. $\bar{\Phi}_{\tau\Lambda}^p(\gamma, \chi; \rho_\xi)$ will be written as $\Phi_{\tau\Lambda}^p(\gamma, \chi; \rho_\xi)$ in the rest of the paper if γ is the first parameter. After discretization of the APH Hamiltonian, H^s is symmetric, because H_γ^r is symmetric, H_V is diagonal, and H_χ is obviously symmetric.

C. Reduction of the H_χ using point group symmetry

If the Hamiltonian H^s of a system commutes with a point group G , i.e., the potential H_V is symmetric under the operations of G , we can reduce the size of the Hamiltonian matrix by transforming the Hamiltonian into the irreducible representations of G .

Let $G = \{R\}$, where $\{R\}$ is a set of symmetry operations such as rotations and reflections. The order of G is h , i.e. G contains h symmetry operations, R . Suppose H_χ satisfies the following eigenequation:

$$H_\chi \phi^{[z, \kappa]}(\chi) = \lambda \phi^{[z, \kappa]}(\chi), \quad (23)$$

where $\phi^{[z, \kappa]}$ transform according the κ th column of the z th irreducible representation of G , i.e., $\phi^{[z, \kappa]}$ is the κ th basis function for the z th irreducible representation, and λ is the corresponding eigenvalue. We will discretize Eq. (23) using a uniform grid

$$\chi_j = (j - 1/2)\Delta\chi, \quad j = 1, hN_\chi, \quad (24)$$

where hN_χ is the number of grid points, $\Delta\chi = 2\pi/hN_\chi$ is the spacing between consecutive grid points, and clearly N_χ is the number of grid points in the interval $[0, 2\pi/h]$. Then, Eq. (23) can be written as

$$\sum_{j=1}^{hN_\chi} H_\chi(\chi_i, \chi_j) \phi^{[z, \kappa]}(\chi_j) = \lambda \phi^{[z, \kappa]}(\chi_i), \quad \kappa = 1, l_z, \quad (25)$$

where l_z is the dimension of the z th irreducible representation. The full range of χ can be generated by applying each symmetry operation R on the range $[1, N_\chi]$. We can then write Eq. (25) as

$$\sum_{j=1}^{N_\chi} \sum_R H_\chi(\chi_i, R\chi_j) \phi^{[z, \kappa]}(R\chi_j) = \lambda \phi^{[z, \kappa]}(\chi_i), \quad \kappa = 1, l_z. \quad (26)$$

From the well-known relations,³⁰

$$\phi^{[z, \kappa]}(R^{-1}\chi) = \sum_{\kappa'} \phi^{[z, \kappa']}(R\chi) \Gamma_{\kappa', \kappa}^{[z]}(R), \quad (27)$$

where $\Gamma_{\kappa', \kappa}^{[z]}(R)$ is the (κ', κ) -th element of the z th irreducible representation matrix of R , we have

$$\begin{aligned} \phi^{[z, \kappa]}(R\chi) &= \sum_{\kappa'} \phi^{[z, \kappa']}(R\chi) \Gamma_{\kappa', \kappa}^{[z]}(R^{-1}) \\ &= \sum_{\kappa'} \phi^{[z, \kappa']}(R\chi) \Gamma_{\kappa', \kappa}^{[z]\dagger}(R) \\ &= \sum_{\kappa'} \phi^{[z, \kappa']}(R\chi) \Gamma_{\kappa, \kappa'}^{[z]*}(R). \end{aligned} \quad (28)$$

The following obvious properties of $\Gamma_{\kappa',\kappa}^{[z]}(R)$ are used in the above derivation, $\Gamma^{[z]}(R^{-1}) = \Gamma^{[z]\dagger}(R) = \Gamma^{[z]-1}(R)$. Substituting Eq. (28) into Eq. (26) we obtain

$$\sum_{j=1}^{N_\chi} \sum_R H_\chi(\chi_i, R\chi_j) \sum_{\kappa'} \phi^{[z,\kappa']}(\chi_j) \Gamma_{\kappa,\kappa'}^{[j]*}(R) = \lambda \phi^{[z,\kappa]}(\chi_i), \quad \kappa = 1, I_z. \quad (29)$$

The expression Eq. (29) is a set of coupled equations which can be written concisely in matrix form. For triatomic reactions, the relevant irreducible representations are either one-dimensional or two-dimensional. For the one-dimensional case, $\kappa = \kappa' = 1$, so we simply omit them. Hence, we have

$$\sum_{j=1}^{N_\chi} H_\chi^r(\chi_i, \chi_j) \phi^{[z]}(\chi_j) = \lambda \phi^{[z]}(\chi_i), \quad (30)$$

where

$$H_\chi^r(\chi_i, \chi_j) = \sum_R H_\chi(\chi_i, R\chi_j) \Gamma^{[z]*}(R), \quad (31)$$

is the reduced H_χ in a one-dimensional irreducible representation.

For the two-dimensional case, we have

$$\sum_{j=1}^{N_\chi} H_\chi^r(\chi_i, \chi_j) \begin{pmatrix} \phi^{[z,1]}(\chi_j) \\ \phi^{[z,2]}(\chi_j) \end{pmatrix} = \lambda \begin{pmatrix} \phi^{[z,1]}(\chi_i) \\ \phi^{[z,2]}(\chi_i) \end{pmatrix}, \quad (32)$$

where

$$H_\chi^r(\chi_i, \chi_j) = \sum_R H_\chi(\chi_i, R\chi_j) \Gamma^{[z]*}(R) \quad (33)$$

is the reduced H_χ in a two-dimensional irreducible representation. It has the same form as in the one-dimensional case, but it is a 2×2 matrix. H_χ^r is symmetric if the associated irreducible representation matrices are real (see Appendix A). There are three types of triatomic interactions: The first type occurs when all atoms are distinct, [ABC]. The point group corresponding to this type is $G = C_2$. The second type occurs when two atoms are identical, [AAB]. The point group corresponding to this type is $G = C_{2v}$. The third type occurs when all atoms are identical, [AAA]. The point group corresponding to this type is $G = C_{6v}$. For all the above groups, G , in each type the irreducible representation matrices are all real, so H_χ^r is symmetric. We provide the representation matrices in Appendix B for convenience.

One should note that if we confine χ to $[0, 2\pi/[G]]$, where $[G]$ is the order of the group, G , H_χ^r is a $N_\chi \times N_\chi$ matrix in a one-dimensional irreducible representation and a $2N_\chi \times 2N_\chi$ matrix in a two-dimensional irreducible representation. When the eigensystem of Eq. (30) or Eq. (32) is solved, eigenfunctions in the range $[0, 2\pi/[G]]$ are obtained. One can employ Eq. (27) to compute the eigenfunctions on the full range of χ .

One can see that using H_χ^r instead of H_χ doesn't affect the symmetrization of H in Sec. III B. Hence, we shall use the following definition of H^s in the rest of this paper:

$$H^s = \frac{\hbar^2}{2\mu\rho_\xi^2} \left[H_\gamma^r + \frac{1}{\sin^2\theta} H_\chi^r \right] + H_V. \quad (34)$$

The derivation presented here may be contrasted with the symmetry-adaptation procedure provided in Ref. 25. In Ref. 25 the symmetry adaptation was carried out by projection of the Hamiltonian (or the derivative operator) onto two different sets of projectors, one on each side of the Hamiltonian matrix. This is useful for cases where the Hamiltonian (or the derivative operator) changes the symmetry of the function it acts on (for example, as in the case of the d/dx operator). In the present case, the symmetry adaptation introduced in this section is only used to adapt the χ part of the Hamiltonian, which is totally symmetric and hence does not change the symmetry of the functions it acts on (unlike the operator corresponding to the θ part).

D. Reduction of the Hamiltonian using projection

Suppose we discretize H^s using N_χ grid points in χ coordinate and N_γ in γ . The size of the Hamiltonian matrix ($N_\gamma N_\chi \times N_\gamma N_\chi$) to be diagonalized is very large for systems of physical interest when highly accurate eigenvalues and eigenfunctions are needed. Since we wish to obtain only a few of the lowest eigenstates to high accuracy, we consider here a projection technique to reduce the size of the Hamiltonian matrix, which leads to a reduction in the CPU time and memory requirements. First, we find a nearly complete basis for the desired lowest eigenvectors, and then we project the Hamiltonian matrix onto this subspace: $H^{\text{cut}} = \tilde{P} H^s P$, where P is the projection matrix and \tilde{P} is the transpose of P . The matrix H^{cut} is small. We solve the eigensystem of H^{cut} and map it back to the original basis to obtain the approximate eigensystem of the H . Details are given below.

Noting that H_γ^r depends only on γ and $\hbar^2/2\mu\rho_\xi^2$ is a constant, and introducing the identity matrices I_γ and I_χ in the γ and χ spaces, respectively, we can rewrite the Hamiltonian H^s in Eq. (34) in the tensor product form

$$H^s = \frac{\hbar^2}{2\mu\rho_\xi^2} H_\gamma^r \otimes I_\chi + \left[\frac{\hbar^2}{2\mu\rho_\xi^2} \frac{1}{\sin^2\theta} I_\gamma \otimes H_\chi^r + H_V I_\gamma \otimes I_\chi \right]. \quad (35)$$

Now H^s is divided into two terms

$$H_1^s = \frac{\hbar^2}{2\mu\rho_\xi^2} H_\gamma^r \otimes I_\chi, \quad (36)$$

$$H_2^s = \frac{\hbar^2}{2\mu\rho_\xi^2} \frac{1}{\sin^2\theta} I_\gamma \otimes H_\chi^r + H_V I_\gamma \otimes I_\chi. \quad (37)$$

The first term, H_1^s , is independent of χ , while the second term depends on both γ and χ . Since we are only interested in the lowest eigenvalues and eigenfunctions of H^s , and H_1^s is independent of χ , one can expect to get accurate results using only a subspace of H_2^s instead. We solve the eigensystem of H_2^s for each fixed γ_j , $H_2^s(\gamma_j) \alpha_k^{\gamma_j} = \lambda_k^{\gamma_j} \alpha_k^{\gamma_j}$, where $(j=1, N_\gamma)$ and N_γ is the number of the grid points used in γ and $(\lambda_k^{\gamma_j}, \alpha_k^{\gamma_j})$ is the k th eigenpair for the given γ_j . Then, we discard the eigenvectors with large eigenvalues. The rest of the eigenvectors consist of a nearly complete basis for the lowest eigenvectors of H^s . In our implementation, we sort all the eigenvectors obtained above in ascending order of eigenvalues, and choose only a number of the

eigenvectors corresponding to the smallest eigenvalues. After normalization we construct the block-diagonal projection matrix, $P_{i,i} = P_i = (\alpha_1^{\gamma_i}, \alpha_2^{\gamma_i}, \dots, \alpha_{m_{\gamma_i}}^{\gamma_i})$.

Because P is an orthonormal, nearly complete basis for the lowest eigenvectors, $\bar{\Phi}_{\tau\Lambda}^p(\gamma, \chi; \rho_\xi)$, we have $P\bar{P}\bar{\Phi}_{\tau\Lambda}^p(\gamma, \chi; \rho_\xi) \approx \bar{\Phi}_{\tau\Lambda}^p(\gamma, \chi; \rho_\xi)$. Substituting $\bar{\Phi}_{\tau\Lambda}^p(\gamma, \chi; \rho_\xi)$ in Eq. (21) and multiplying by \bar{P} from the left, we get $H^{\text{cut}}\Psi_{\tau\Lambda}^p(\gamma, \chi; \rho_\xi) \approx \mathcal{E}_{\tau\Lambda}^p(\rho_\xi)\Psi_{\tau\Lambda}^p(\gamma, \chi; \rho_\xi)$, where $H^{\text{cut}} = \bar{P}HP$ and $\Psi_{\tau\Lambda}^p(\gamma, \chi; \rho_\xi) = \bar{P}\bar{\Phi}_{\tau\Lambda}^p(\gamma, \chi; \rho_\xi)$. We can see that P is an $N_\gamma N_\chi \times N_\chi^{\text{cut}}$ matrix, where $N^{\text{cut}} = \sum_{i=1}^{N_\gamma} m_{\gamma_i}$ so H^{cut} is an $N^{\text{cut}} \times N^{\text{cut}}$ matrix. Its size is much smaller than the size of H^s if N^{cut} is much smaller than $N_\gamma N_\chi$, which is the case if we want only a few eigenvalues. N^{cut} should be taken to be as small as possible, consistent with the desired level of convergence. Noting that H^s is symmetric, we have $\bar{H}^{\text{cut}} = \bar{P}\bar{H}^s P = \bar{P}H^s P = H^{\text{cut}}$. Thus, H^{cut} is symmetric.

IV. NUMERICAL TESTS

Numerical tests are carried out to study three aspects of the approach. First, we test the behavior with respect to parameter M in the PDAF $\delta_{p,M}^{(k)}$. Next, we examine the H_χ^r using different irreducible representations of various groups. Finally, the accuracy of H_χ^r is tested.

A. Test of PDAFs

We tested PDAFs using different periodic functions, all of them showing similar results. Here, we present only the test for the eigenvalues of H_χ . Using the PDAF matrix defined in Eq. (10) we obtain the discrete representation of H_χ

$$H_{\chi_{ij}} = - \sum_{k=1}^{N_\chi} D_{ij}^{(2)} = - \sum_{k=1}^{N_\chi} \delta_{p,M}^{(2)}(\chi_i - \chi_j) \Delta\chi, \quad (38)$$

where N_χ is the number of grid points used in $(0, 2\pi)$, $\Delta\chi = 2\pi/N_\chi$ and $\chi_j = (j - \frac{1}{2})\Delta\chi$. We know that the correct eigenvalues of H_χ should be $0, 1, 1, 4, 4, \dots, k^2, k^2, \dots$, so it's easy to check the difference between the computed eigenvalues and the exact ones. We set the criterion of 10^{-6} as the maximum tolerable error and then count how many good eigenvalues can be obtained. A typical result is shown in Fig. 3, in which we set $N_\chi = 32$ and various M from 1 to 35. One can see that when $M = N_\chi/2$, almost all eigenvalues are good. This suggests the optimal choice of M .

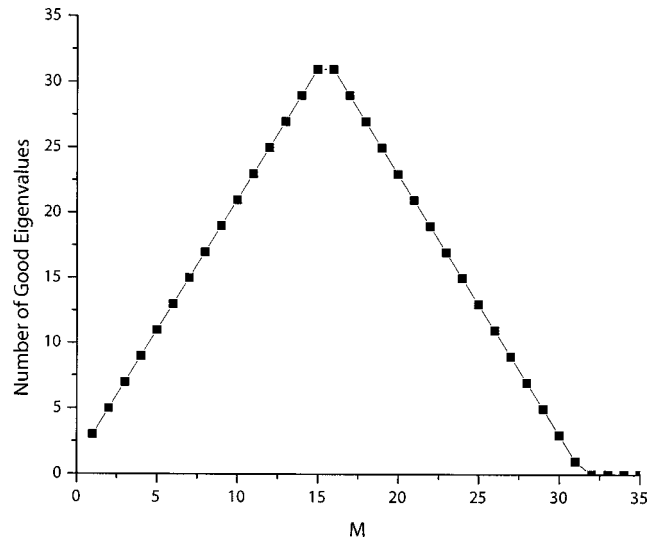


FIG. 3. The number of good eigenvalues reaches maximum when $M = N_\chi/2$ ($N_\chi = 32$), where M is the parameter in PDAF $\delta_{p,M}^{(k)}(x)$, and N_χ is the number of grid points in range $(0, 2\pi)$.

B. Test of H_χ^r

Tests of H_χ^r were done for all the aforementioned irreducible representations of the relevant point groups. All of them give good results. Here, we present only one typical result computed using the C_{2v} group, since only C_{2v} is involved in the FH_2 reaction calculation. We chose the $\text{F} + \text{H}_2$ system, since we have published detailed convergence studies using the DVR and the ABM methods.

Similar to H_χ , we can obtain the PDAF representation of H_χ^r . Note that C_{2v} has only one-dimensional irreducible representations, so we use Eq. (31) for H_χ^r . We obtain the discrete representation of H_χ^r as

$$H_{\chi_{ij}} = - \sum_{k=1}^{N_\chi} \sum_R \delta_{p,M}^{(2)}(\chi_i - R\chi_j) \Gamma^{[z]} \Delta\chi. \quad (39)$$

Note that the grid scheme is defined in Eq. (24). We set $N_\chi = 8$, and the eigenvalues λ_k for each of the irreducible representations are computed, and the $\sqrt{\lambda_k}$ are shown in Table I for easy comparison. One can see that if we combine the results from all the irreducible representations, we will obtain the (approximate) eigenvalues $0, 1, 1, 4, 4, \dots, k^2, k^2, \dots$, which are obtained from H_χ . We also note that the degenerate eigenvalues in H_χ are no longer degenerate in H_χ^r .

TABLE I. $\sqrt{\lambda_k}$, square roots of eigenvalues of H_χ^r in irreducible representations of group C_{2v} .

k	A_1	B_1	A_2	B_2
1	0.000 000 524 560 66	2.000 000 000 000 09	0.999 999 999 999 89	1.000 000 000 000 07
2	2.000 000 000 000 07	3.999 999 999 999 97	3.000 000 000 000 04	3.000 000 000 000 02
3	3.999 999 999 999 99	5.999 999 999 999 99	5.000 000 000 000 00	5.000 000 000 000 00
4	5.999 999 999 999 99	7.999 999 999 999 99	7.000 000 000 000 00	7.000 000 000 000 00
5	7.999 999 999 999 99	10.000 000 000 000 0	9.000 000 000 000 01	9.000 000 000 000 01
6	10.000 000 000 000 0	12.000 000 000 000 0	11.000 000 000 000 0	11.000 000 000 000 0
7	12.000 000 000 000 0	14.000 000 000 000 0	13.000 000 000 000 0	13.000 000 000 000 0
8	14.000 000 000 000 0	22.627 416 997 969 5	15.000 000 000 000 0	15.000 000 000 000 0

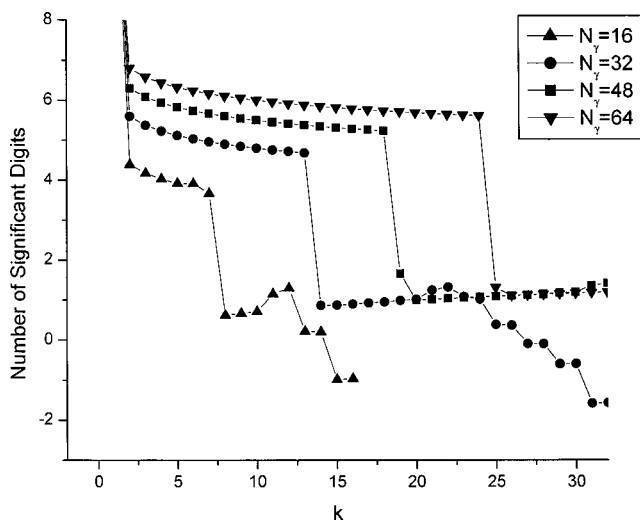


FIG. 4. Accuracy (number of significant digits) in eigenvalues of H_γ^r . For all N_γ , the smallest $N_\gamma/3$ eigenvalues are of high accuracy.

C. Test of H_γ^r

H_γ^r in Eq. (19) has the same eigenvalues as H_θ . If we rewrite H_θ as

$$H_\theta = -\frac{8}{\sin 2\theta} \frac{\partial}{\partial 2\theta} \sin 2\theta \frac{\partial}{\partial 2\theta}, \quad (40)$$

we can see that the eigenequation of $H_\theta \psi(\theta) = \lambda \psi(\theta)$ is a Legendre differential equation if we write the eigenvalue as $\lambda_l = 8l(l+1)$ $l=0,1,\dots$. Thus, H_γ^r has eigenvalues of $8l(l+1)$. To evaluate the accuracy of the computed eigenvalue, we define $S_l(\lambda_l)$ as, $S_l(\lambda_l) = -\lg[|\lambda_l - 8l(l+1)|/|8l(l+1)|]$, where λ_l is the l th computed eigenvalue, and $S_l(\lambda_l)$ gives the approximate number of significant digits. Figure 4 shows the results when we set $N_\gamma = 16, 32, 48$, and 64. One can see that for each N_γ there are about $N_\gamma/3$ eigenvalues of high accuracy. This is accurate enough for the FH_2 calculation, because typically the order of the Hamiltonian matrix is about 1000, but we require less than 300 eigenvalues.

It is worth mentioning that we also tested the nonsymmetric form, H_θ , using the PDAF presentation. Although we can get as highly accurate results from either H_χ or H_χ^r , we still choose the symmetric form, because the nonsymmetric matrix costs more time and memory to diagonalize. Moreover, when we add the potential, the accuracy of the nonsymmetric form will decrease to the accuracy of the symmetric H_γ^r .

V. CALCULATIONS FOR THE FH_2 SYSTEM

In this section we report the results of PDAF calculations of surface functions and the matrix elements, and compare them with the results of the DVR and ABM methods. The system chosen as a nontrivial example is the $\text{F} + \text{H}_2 \rightarrow \text{HF} + \text{H}$ reaction; its treatment requires generation of a large basis of surface functions. The potential energy surface (PES) used is that of Brown *et al.*²⁹ commonly called the T5A surface, and we choose the zero of energy to be at the bottom of the asymptotic HF potential wells. This PES has been used in many calculations^{8,14,20,28,31-34} on this reaction,

and plots of the PES and surface functions showing their appearance in APH coordinates have also been published. Arrangement 1 or i(initial) is taken to be $\text{F} + \text{H}_2$ reactants. Detailed convergence studies have been published for $\text{F} + \text{H}_2$ using the DVR and ABM methods. For comparison of these methods with the current PDAF method, we use all parameters and methods as outlined in those publications.^{14,24}

The calculations are for $\Lambda=0$ and even parity ($p=0$) and include all functions connecting to the even j rotational states of the $\text{F} + \text{H}_2$ arrangement. Because of the symmetry due to the identical H atoms, this only requires including in the PDAF calculations the A_1 irreducible representation, in which the surface functions are even under reflection about $\chi=0$.

A. Grid size and mapping

The grid sizes (the number of grid points), N_χ , N_γ , and N^{cut} are determined by the convergence test. We present only the results here. To attain five significant digits in the lowest 100 eigenvalues for any ρ_ξ , we use $N_\gamma = [25.852 + 5.85119\rho_\xi - 0.130102\rho_\xi^2 - 0.0042517\rho_\xi^3]$, $N^{\text{cut}} = [1428.06 + 29.2007\rho_\xi - 6.37755\rho_\xi^2 - 0.119048\rho_\xi^3]$, and $N_\chi = [4\pi \max(N_\gamma)]/[G]$, where $[G]$ is the order of the associated symmetry group. To get N_χ , we use the maximum of N_γ because it makes N_χ identical for all ρ_ξ , thus making it easy to compute the overlap matrices. Also, using the maximum N_γ doesn't significantly increase the computation time, because we reduce the matrix size according to N^{cut} , as discussed in Sec. III D.

Although N_χ is chosen to be the same for all ρ_ξ , N_γ is different. Hence, before we compute the overlap matrix, we have to map the wave functions to a uniform grid, to reduce the computation time for the overlap matrix.

Let N_γ^u be the number of uniform grid points in γ , N_γ is the original number of grid points. Applying Eq. (8) to the wave function

$$\begin{aligned} \Phi_{\tau\Lambda}^p(\gamma_j, \chi; \rho_\xi) &= \sum_{k=1}^{2N_\gamma} \delta_{p,M}(\gamma_j - \gamma_k) \Phi_{\tau\Lambda}^p(\gamma_k, \chi; \rho_\xi) \Delta\gamma \\ &= \sum_{k=1}^{N_\gamma} [\delta_{p,M}(\gamma_j - \gamma_k) + \delta_{p,M}(\gamma_j - 2\pi + \gamma_k)] \\ &\quad \times \Phi_{\tau\Lambda}^p(\gamma_k, \chi; \rho_\xi) \Delta\gamma, \end{aligned} \quad (41)$$

TABLE II. PDAF, ABM, DVR, and FEM surface function energies \mathcal{E}_τ and average energies in eV at $\rho = 2.2 a_0$.

τ	PDAF	ABM	DVR	FEM
1	6.9176	6.9177	6.9177	6.9177
2	7.0341	7.0341	7.0341	7.0342
3	7.1299	7.1298	7.1296	7.1299
4	7.3044	7.3042	7.3038	7.3043
5	7.4934	7.4932	7.4927	7.4933
6	7.7007	7.7007	7.7008	7.7009
7	7.9227	7.9219	7.9202	7.9222
8	8.0786	8.0789	8.0786	8.0791
9	8.1548	8.1524	8.1475	8.1529
10	8.2495	8.2502	8.2494	8.2503
$\bar{\mathcal{E}}(10)$	7.5986	7.5983	7.5974	7.5985

TABLE III. PDAF, ABM, DVR, and FEM surface function energies \mathcal{E}_τ and average energies in eV at $\rho=3.037\,582\,8\,a_0$.

τ	PDAF	ABM	DVR	FEM
11	1.9845	1.9845	1.9845	1.9849
12	1.9975	1.9975	1.9975	1.9979
13	2.0514	2.0515	2.0515	2.0519
14	2.1090	2.1090	2.1090	2.1093
15	2.1275	2.1275	2.1275	2.1281
16	2.1352	2.1352	2.1353	2.1357
17	2.1993	2.1994	2.1994	2.1998
18	2.2578	2.2578	2.2578	2.2584
19	2.2730	2.2730	2.2730	2.2737
20	2.3197	2.3197	2.3197	2.3204
$\bar{\mathcal{E}}(20)$	1.8551	1.8551	1.8551	1.8554

where $\Delta\gamma = \pi/N_\gamma$, and γ_j, γ_k represent the coordinates in the above two grid schemes, respectively, $\gamma_j = (j - \frac{1}{2})\Delta\gamma^u$, and $\gamma_k = (k - \frac{1}{2})\Delta\gamma$, where $\Delta\gamma^u = \pi/N_\gamma^u$.

B. Eigenvalues

The atomic masses used are mass of F = 18.998 403 2 a.u., and mass of H = 1.007 825 03 a.u. The calculations were performed at five representative ρ values ranging from the smallest to the largest values that were needed in our reactive scattering calculations.^{14,20} The precise values of ρ chosen have no particular significance, and some were chosen simply because the convergence of the DVR method had already been studied at these values.^{14,24}

The results are given in Tables II–VI for the five values of ρ chosen. In each table, the energy eigenvalues of the highest ten important or open surface function states are given in eV. The omitted lower eigenvalues always agree to more significant figures than those shown. Also shown is $\bar{\mathcal{E}}(n)$, the average of the first n eigenvalues. This gives a convenient measure of the overall agreement of the methods.

C. Matrix elements

The APH surface functions $\Phi_{\tau\Lambda}^p(\gamma, \chi; \rho_\xi)$ are “sector adiabatic” or “diabatic-by-sector;” that is, they change from sector to sector, but are independent of ρ within a sector.

TABLE IV. PDAF, ABM, DVR, and FEM surface function energies \mathcal{E}_τ and average energies in eV at $\rho=4.974\,796\,6\,a_0$.

τ	PDAF	ABM	DVR	FEM
91	2.0699	2.0701	2.0701	2.0720
92	2.0721	2.0734	2.0727	2.0760
93	2.0864	2.0896	2.0869	2.0916
94	2.0941	2.0941	2.0943	2.0961
95	2.1087	2.1107	2.1093	2.1132
96	2.1215	2.1232	2.1220	2.1267
97	2.1487	2.1509	2.1495	2.1549
98	2.1643	2.1650	2.1645	2.1672
99	2.1793	2.1806	2.1799	2.1833
100	2.1892	2.1892	2.1893	2.1918
$\bar{\mathcal{E}}(100)$	1.3974	1.3977	1.3975	1.3985

TABLE V. PDAF, ABM, DVR, and FEM surface function energies \mathcal{E}_τ and average energies in eV at $\rho=7.298\,999\,3\,a_0$.

τ	PDAF	ABM	DVR	FEM
91	2.0559	2.0564	2.0569	2.0679
92	2.0749	2.0754	2.0760	2.0928
93	2.0980	2.0981	2.0981	2.1023
94	2.0985	2.0990	2.0994	2.1141
95	2.1098	2.1098	2.1099	2.1148
96	2.1194	2.1196	2.1198	2.1278
97	2.1268	2.1273	2.1278	2.1443
98	2.1538	2.1542	2.1543	2.1537
99	2.1551	2.1551	2.1551	2.1608
100	2.1597	2.1602	2.1608	2.1621
$\bar{\mathcal{E}}(100)$	1.3788	1.3788	1.3790	1.3811

Thus, when the APH wave function is substituted into the Schrödinger equation, the resulting exact coupled channel or close-coupling equations are of the form⁹

$$\left[\frac{\partial^2}{\partial \rho^2} + \frac{2\mu E}{\hbar^2} \right] \psi_{\tau\Lambda}^{Jp_n}(\rho) = \frac{2\mu}{\hbar^2} \sum_{\tau'\Lambda'} \langle \Phi_{\tau\Lambda}^{Jp} \hat{D}_{\Lambda M}^{Jp} | H_i | \Phi_{\tau'\Lambda'}^{Jp} \hat{D}_{\Lambda' M'}^{Jp} \rangle \psi_{\tau'\Lambda'}^{Jp_n}(\rho). \quad (42)$$

The matrix elements are obtained in Ref. 9 as

$$\begin{aligned} & \langle \Phi_{\tau\Lambda}^{Jp} \hat{D}_{\Lambda M}^{Jp} | H_i | \Phi_{\tau'\Lambda'}^{Jp} \hat{D}_{\Lambda' M'}^{Jp} \rangle \\ &= \frac{\rho_\xi^2}{\rho^2} \mathcal{E}_{\tau\Lambda}(\rho_\xi) \delta_{\tau\tau'} \delta_{\Lambda\Lambda'} + \delta_{\Lambda\Lambda'} \\ & \times \langle \Phi_{\tau\Lambda}^{Jp} | V(\rho, \theta, \chi) - \frac{\rho_\xi^2}{\rho^2} V(\rho_\xi, \theta, \chi) | \Phi_{\tau'\Lambda'}^{Jp} \rangle \\ & + \langle \Phi_{\tau\Lambda}^{Jp} \hat{D}_{\Lambda M}^{Jp} | \frac{A-B}{2} (J_x^2 - J_y^2) + T_c | \Phi_{\tau'\Lambda'}^{Jp} \hat{D}_{\Lambda' M'}^{Jp} \rangle, \quad (43) \end{aligned}$$

where ρ_ξ denotes the ξ th hyper-radius sampled from the interval $[\rho_{\min}, \rho_{\max}]$. The ρ_ξ are given by $\rho_\xi = [\rho_{\min} + (\xi - 1)\Delta\rho_1](1 + \Delta\rho_2)^{\xi-1}$. This algorithm spaces the sector centers logarithmically. Given a sector with sector center ρ_ξ , we evaluate matrix elements at the three rho values given by $\rho_1 = (\rho_{\xi-1} + \rho_\xi)/2$, $\rho_2 = \rho_\xi$, and $\rho_3 = (\rho_\xi + \rho_{\xi+1})/2$. All the

TABLE VI. PDAF, ABM, DVR, and FEM surface function energies \mathcal{E}_τ and average energies in eV at $\rho=9.0a_0$.

τ	PDAF	ABM	DVR	FEM
91	2.0747	2.0747	2.0748	2.0805
92	2.0774	2.0779	2.0782	2.0863
93	2.0957	2.0964	2.0974	2.1051
94	2.1010	2.1010	2.1009	2.1065
95	2.1153	2.1153	2.1154	2.1233
96	2.1189	2.1194	2.1197	2.1284
97	2.1250	2.1252	2.1253	2.1315
98	2.1461	2.1470	2.1482	2.1541
99	2.1542	2.1545	2.1546	2.1562
100	2.1558	2.1559	2.1560	2.1564
$\bar{\mathcal{E}}(100)$	1.3791	1.3791	1.3792	1.3812

matrix elements in Eq. (43) are independent of E , so that they can be calculated once, stored, and used at many scattering energies.

The wave functions $\Phi_{\tau\Lambda}^p(\gamma, \chi; \rho_\xi)$ should be normalized before computation of the matrix elements. The normalization factor N can be calculated in the desired irreducible representation easily according to Eq. (13) as shown below

$$\begin{aligned} 1 &= N \int_0^{2\pi} d\chi \int_0^{\pi/2} d\theta \sin 2\theta \Phi_{\tau\Lambda}^p{}^2(\theta, \chi; \rho_\xi) \\ &= N \int_0^{2\pi} d\chi \int_0^\pi d\gamma \frac{\pi}{4} \sin \gamma \sin 2\theta \Phi_{\tau\Lambda}^p{}^2(\gamma, \chi; \rho_\xi) \\ &= hN \sum_{i=1}^{N_\chi} \sum_{j=1}^{N_\gamma} \Delta\chi \Delta\gamma \frac{\pi}{4} \sin \gamma_j \sin 2\theta(\gamma_j) \\ &\quad \times \Phi_{\tau\Lambda}^p{}^2(\gamma_j, \chi_i; \rho_\xi). \end{aligned}$$

Thus

$$\begin{aligned} N &= \left\{ \frac{1}{4} h \pi \Delta\chi \Delta\gamma \sum_{i=1}^{N_\chi} \sum_{j=1}^{N_\gamma} \sin \gamma_j \right. \\ &\quad \left. \times \sin 2\theta(\gamma_j) \Phi_{\tau\Lambda}^p{}^2(\gamma_j, \chi_i; \rho_\xi) \right\}^{-1/2}. \end{aligned} \quad (44)$$

After $\Phi_{\tau\Lambda}^p(\gamma, \chi; \rho_\xi)$ is normalized, we compute the matrix elements. The first term on the right-hand side of Eq. (43) is just a local internal energy which, together with the E term on the left-hand side of Eq. (42), determines a local wave number.

The second term of Eq. (42) is often called a potential matrix element. It is small on the sector and can be evaluated with the same quadratures used in getting the surface functions. Similar to the evaluation of the normalization factor, we obtain for the potential matrix elements

$$\begin{aligned} \langle \Phi_{\tau\Lambda}^{Jp}(\rho_\xi) | V(\rho) - \frac{\rho_\xi^2}{\rho^2} V(\rho_\xi) | \Phi_{\tau'\Lambda'}^{Jp}(\rho_\xi) \rangle \\ &= \frac{1}{4} h \pi \Delta\chi \Delta\gamma \sum_{i=1}^{N_\chi} \sum_{j=1}^{N_\gamma} \sin \gamma_j \sin 2\theta(\gamma_j) \\ &\quad \times \Phi_{\tau\Lambda}^p(\gamma_j, \chi_i; \rho_\xi) \left[V(\rho) - \frac{\rho_\xi^2}{\rho^2} V(\rho_\xi) \right] \\ &\quad \times \Phi_{\tau'\Lambda'}^p(\gamma_j, \chi_i; \rho_\xi). \end{aligned} \quad (45)$$

The Coriolis term can be simplified as

$$\begin{aligned} \langle \Phi_{\tau\Lambda}^{Jp} \hat{D}_{\Lambda M}^{Jp} | T_c | \Phi_{\tau'\Lambda'}^{Jp} \hat{D}_{\Lambda' M'}^{Jp} \rangle \\ &= \frac{-\hbar^2}{2\mu\rho^2} \langle \Phi_{\tau\Lambda}^p | \frac{\cos \theta}{\sin^2 \theta} \frac{\partial}{\partial \chi} | \Phi_{\tau'\Lambda'}^p \rangle \\ &\quad \times [(1 + \delta_{\Lambda 0})(1 + \delta_{\Lambda' 0})]^{-1/2} \\ &\quad + [\lambda_-(J, \Lambda)(-1)^{J+\Lambda+p} \delta_{\Lambda', \Lambda-1}], \end{aligned} \quad (46)$$

where $\lambda_\pm(J, \Lambda) = \sqrt{[(J \pm \Lambda + 1)(J \mp \Lambda)]}$ and

$$\begin{aligned} \langle \Phi_{\tau\Lambda}^p | \frac{\cos \theta}{\sin^2 \theta} \frac{\partial}{\partial \chi} | \Phi_{\tau'\Lambda'}^p \rangle \\ &= \frac{1}{2} h \pi \Delta\chi \Delta\gamma \sum_{i=1}^{N_\chi} \sum_{j=1}^{N_\gamma} \sum_{k=1}^{N_\chi} \sin \gamma_j \frac{\cos^2 \theta(\gamma_j)}{\sin \theta(\gamma_j)} \\ &\quad \times \Phi_{\tau\Lambda}^p(\gamma_j, \chi_i; \rho_\xi) \delta_{p,M}^{(1)}(\chi_i - \chi_k) \Phi_{\tau'\Lambda'}^p(\gamma_j, \chi_k; \rho_\xi). \end{aligned} \quad (47)$$

It should be noted that the last term in the bracket in Eq. (47) is nonzero only when $\Lambda = 0$ or 1 , and also that because the ρ dependence of the operator factors out, the matrix elements over the $\Phi_{\tau\Lambda}^p(\gamma, \chi; \rho_\xi)$ only need to be evaluated once on each sector. They are readily evaluated using the PDAF $\Phi_{\tau\Lambda}^p(\gamma, \chi; \rho_\xi)$ at the quadrature points since the PDAF code generates the derivatives of $\Phi_{\tau\Lambda}^p(\gamma, \chi; \rho_\xi)$ directly.

The asymmetric top terms of Eq. (43) can be explicitly written as

$$\begin{aligned} \langle \tau\Lambda | \frac{1}{2}(A - B)(J_x^2 - J_y^2) | \tau'\Lambda' \rangle \\ &= \frac{1}{4} \hbar^2 \langle \Phi_{\tau\Lambda}^p | A - B | \Phi_{\tau'\Lambda'}^p \rangle [(1 + \delta_{\Lambda 0})(1 + \delta_{\Lambda' 0})]^{-1/2} \\ &\quad \times [\lambda_+(J, \Lambda) \lambda_+(J, \Lambda + 1) \delta_{\Lambda', \Lambda+2} \\ &\quad \times \lambda_-(J, \Lambda) \lambda_-(J, \Lambda - 1) \delta_{\Lambda', \Lambda-2} \\ &\quad + (-1)^{J+\Lambda+p} \lambda_-(J, \Lambda) \lambda_-(J, \Lambda - 1) \delta_{\Lambda', 2-\Lambda}], \end{aligned} \quad (48)$$

where $A = 1/\mu\rho_\xi^2(1 + \sin^2 \theta)$, $B = 1/2\mu\rho_\xi^2 \sin^2 \theta$, and

$$\begin{aligned} \langle \Phi_{\tau\Lambda}^p | A - B | \Phi_{\tau'\Lambda'}^p \rangle \\ &= \frac{1}{4} h \pi \Delta\chi \Delta\gamma \sum_{i=1}^{N_\chi} \sum_{j=1}^{N_\gamma} \sin \gamma_j \sin 2\theta(\gamma_j) \\ &\quad \times \Phi_{\tau\Lambda}^p(\gamma_j, \chi_i; \rho_\xi) (A - B) \Phi_{\tau'\Lambda'}^p(\gamma_j, \chi_i; \rho_\xi). \end{aligned}$$

The third term in the bracket in Eq. (43) is always zero if $|\Lambda - \Lambda'| > 2$, and the ρ dependence of $A - B$ again factors out, giving the same simplifications and allowing the evaluation of the integrals by the same methods as for the Coriolis terms.

At the boundaries between sectors, the R matrix is transformed by an orthogonal transformation, which requires calculation of the overlap matrix elements. The formula for the overlap matrix elements is given by

$$\begin{aligned} \langle \Phi_{\tau\Lambda}^{Jp}(\rho_\xi) | \Phi_{\tau'\Lambda'}^{Jp}(\rho_{\xi'}) \rangle \\ &= \frac{1}{4} h \pi \Delta\chi \Delta\gamma \sum_{i=1}^{N_\chi} \sum_{j=1}^{N_\gamma} \frac{\pi}{4} \sin \gamma_j \sin 2\theta(\gamma_j) \\ &\quad \times \Phi_{\tau\Lambda}^{Jp}(\gamma_j, \chi_i; \rho_\xi) \Phi_{\tau'\Lambda'}^{Jp}(\gamma_j, \chi_i; \rho_{\xi'}). \end{aligned} \quad (49)$$

D. Comparison of methods

We compare the computational efficiency of the PDAF, DVR, ABM, and FEM methods on the same computer (PIII 866 MHz), by computing eigenvalues, potential matrix elements, and overlap matrices at $100 \rho_\xi$'s. ρ_ξ starts from $2.0 a_0$

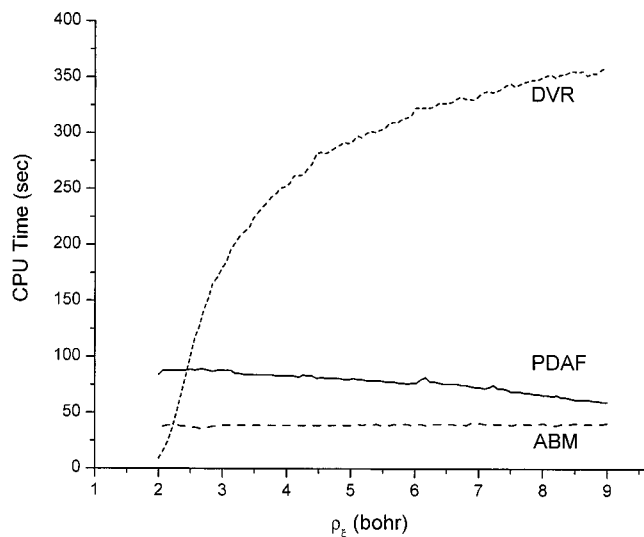


FIG. 5. CPU time of PDAF, DVR, and ABM.

and ends at $9.0a_0$ and is evenly spaced in between. The computation times (CPU time) are shown in Fig. 5.

The FEM method takes much more time than the others; thus, we do not include it in Fig. 5. We see that the PDAF method is much faster than the DVR over most of the range of ρ_ξ . If ρ_ξ is very small (less than $2.2a_0$), the DVR is the most efficient method. Although the ABM works slightly faster than the PDAF method, it turns out that the ABM diverges when ρ_ξ is small. We have also made comparisons of the three methods for different systems, namely H_2O , HeH_2 , LiFH , H_3 , HO_2 , and $e^+ + \text{H}$. In all cases we see results similar to Fig. 5. The distances where the PDAF is computationally faster than the DVR or ABM method vary considerably from system to system. For the LiFH system the PDAF is more than an order of magnitude faster than the ABM method for distances less than $6.0a_0$. The DVR method is generally faster than the PDAF at relatively short hyper-radii where the wave functions become highly delocalized and the PDAF becomes more efficient at larger hyper-

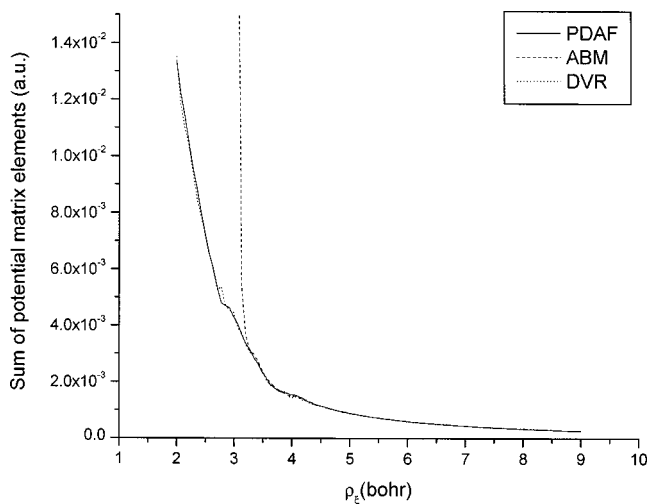


FIG. 6. Comparison of the sum of potential matrix elements using PDAF, ABM, and DVR.

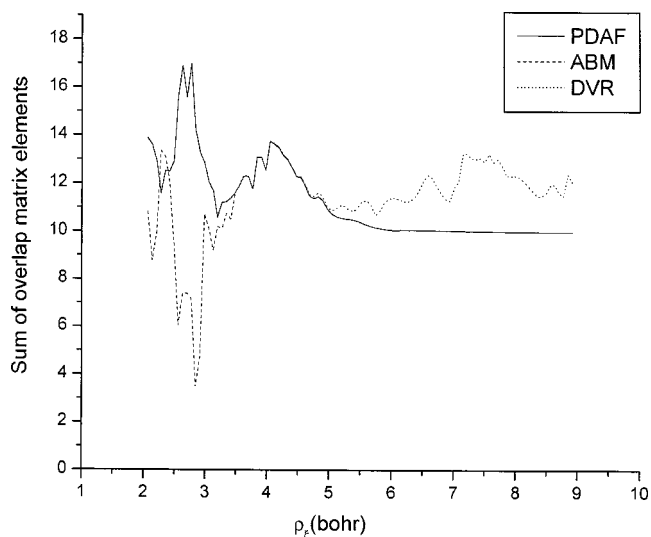


FIG. 7. Comparison of the sum of the overlap matrix elements using PDAF, ABM, and DVR.

radii. However, for the LiFH system the PDAF method is much faster than the DVR at all hyper-radii. For the $e^+ + \text{H}$ system (which has an attractive singularity) the FEM and ABM methods should be used to ensure correct behavior of the surface functions near the singularities. The DVR is an excellent method and should not be discounted. There are situations where the DVR method is definitely faster and more accurate. We used a Legendre DVR and it is possible that a Fourier DVR³⁴ would be more efficient. It should be noted that DVRs and DAFs are intrinsically different. The DVR uses a basis and transforms the basis to a grid which is closely related to that basis. The DAF is an *approximating functional* and is not as likely to ring. Studies are being conducted on simple one-dimensional potentials to determine the circumstances for which each method excels.

We compare only the potential matrix elements and the overlap matrix elements here, computed using the ABM, DVR, and PDAF. The comparison of the potential matrix elements is shown in Fig. 6 and one can see that all three methods agree with each other very well when $\rho > 3.3a_0$. However, when $\rho < 3.3$, the ABM result diverges from the PDAF and DVR significantly. The comparison of the overlap matrix elements is shown in Fig. 7. One can see clearly from the figure that the PDAF gives results very close to the DVR at small ρ ($\rho < 3.4a_0$), and it also agrees with the ABM very well at large ρ ($\rho > 4.4a_0$). The ABM gives very different results from the PDAF and DVR at small ρ , and DVR gives very different results from PDAF and ABM at large ρ . We know that the ABM is very accurate at large ρ and the DVR at small ρ , and thus the comparisons show that the PDAF is accurate both for small and large ρ .

VI. CONCLUSION

In this paper we have presented a periodic distributed approximating functional (PDAF) method for calculating the surface function basis needed in hyper-spherical formulations of reactive scattering theory. PDAF functions are intro-

TABLE VII. Irreducible representations of group C_2 .

C_2 $R\chi$	E χ	C_2 $\pi+\chi$	p
A	1	1	0
B	1	-1	1

duced and shown to be capable of providing an accurate, efficient representation of the derivative operators. The PDAF is efficient for all values of ρ small and large.

Test calculations on the $F+H_2$ system with the T5A PES, comparing the PDAF, ABM, DVR, and FEM methods showed that the FEM is always the least efficient of the four, and the ABM is the most efficient method for large ρ but is not accurate at small ρ . On the other hand, the DVR is the most efficient method for small ρ but is not accurate for large ρ .

ACKNOWLEDGMENTS

One of the authors (G.A.P.) is supported by National Science Foundation Grant Nos. CHE-9710383 and PHY-0100704. D.J.K. is supported by National Science Foundation Grant No. CHE-007431 and R.A. Welsch Foundation

TABLE VIII. Irreducible representations of group C_{2v} .

C_{2v} $R\chi$	E χ	C_2 $\pi+\chi$	σ_v $2\pi-\chi$	σ'_v $\pi-\chi$	p
A_1	1	1	1	1	0
A_2	1	1	-1	1	0
B_1	1	-1	1	-1	1
B_2	1	-1	-1	1	1

Grant No. E-0608. The Ames Laboratory is supported by the U.S. Department of Energy under Contract No. 2-7405-ENG82.

APPENDIX A: H_χ^r IS SYMMETRIC

$$H_\chi^r(\chi_i, \chi_j) = \sum_R H_\chi(\chi_i, R\chi_j) \Gamma^{[\tau]*}(R). \quad (A1)$$

To prove that H_χ^r is symmetric, it is sufficient to show

$$H_\chi^{r, \kappa, \kappa'}(\chi_i, \chi_j) = H_\chi^{r, \kappa', \kappa}(\chi_j, \chi_i), \quad (A2)$$

where

$$H_\chi^{r, \kappa, \kappa'}(\chi_i, \chi_j) = \sum_R H_\chi(\chi_i, R\chi_j) \Gamma_{\kappa, \kappa'}^{[\tau]*}(R). \quad (A3)$$

We know that H_χ is symmetric, so

TABLE IX. Irreducible representations of group C_{6v} .

C_{6v} $R\chi$	E χ	C_6 $\frac{\pi}{3}+\chi$	C_6^5 $\frac{5\pi}{3}+\chi$	C_3 $\frac{2\pi}{3}+\chi$	C_3^2 $\frac{4\pi}{3}+\chi$	C_2 $\pi+\chi$	p
A_1	1	1	1	1	1	1	0
A_2	1	1	1	1	1	1	0
B_1	1	-1	-1	1	1	-1	1
B_2	1	-1	-1	1	1	-1	1
E_1	$\begin{pmatrix} 1 & 0 \\ 0 & 1 \end{pmatrix}$	$\begin{pmatrix} \frac{1}{2} & \frac{\sqrt{3}}{2} \\ \frac{\sqrt{3}}{2} & \frac{1}{2} \end{pmatrix}$	$\begin{pmatrix} \frac{1}{2} & \frac{\sqrt{3}}{2} \\ -\frac{\sqrt{3}}{2} & \frac{1}{2} \end{pmatrix}$	$\begin{pmatrix} -\frac{1}{2} & \frac{\sqrt{3}}{2} \\ \frac{\sqrt{3}}{2} & -\frac{1}{2} \end{pmatrix}$	$\begin{pmatrix} -\frac{1}{2} & \frac{\sqrt{3}}{2} \\ -\frac{\sqrt{3}}{2} & -\frac{1}{2} \end{pmatrix}$	$\begin{pmatrix} -1 & 0 \\ 0 & -1 \end{pmatrix}$	1
E_2	$\begin{pmatrix} 1 & 0 \\ 0 & 1 \end{pmatrix}$	$\begin{pmatrix} -\frac{1}{2} & \frac{\sqrt{3}}{2} \\ \frac{\sqrt{3}}{2} & -\frac{1}{2} \end{pmatrix}$	$\begin{pmatrix} -\frac{1}{2} & \frac{\sqrt{3}}{2} \\ -\frac{\sqrt{3}}{2} & -\frac{1}{2} \end{pmatrix}$	$\begin{pmatrix} -\frac{1}{2} & \frac{\sqrt{3}}{2} \\ \frac{\sqrt{3}}{2} & -\frac{1}{2} \end{pmatrix}$	$\begin{pmatrix} -\frac{1}{2} & \frac{\sqrt{3}}{2} \\ -\frac{\sqrt{3}}{2} & -\frac{1}{2} \end{pmatrix}$	$\begin{pmatrix} 1 & 0 \\ 0 & 1 \end{pmatrix}$	0
R $R\chi$	σ_v $2\pi-\chi$	σ'_v $\frac{2\pi}{3}-\chi$	σ''_v $\frac{4\pi}{3}-\chi$	σ_d $\frac{\pi}{3}-\chi$	σ'_d $\pi-\chi$	σ''_d $\frac{5\pi}{3}-\chi$	p
A_1	1	1	1	1	1	1	0
A_2	-1	-1	-1	-1	-1	-1	0
B_1	1	1	1	-1	-1	-1	1
B_2	-1	-1	-1	1	1	1	1
E_1	$\begin{pmatrix} 1 & 0 \\ 0 & -1 \end{pmatrix}$	$\begin{pmatrix} -\frac{1}{2} & \frac{\sqrt{3}}{2} \\ \frac{\sqrt{3}}{2} & \frac{1}{2} \end{pmatrix}$	$\begin{pmatrix} -\frac{1}{2} & \frac{\sqrt{3}}{2} \\ -\frac{\sqrt{3}}{2} & \frac{1}{2} \end{pmatrix}$	$\begin{pmatrix} \frac{1}{2} & \frac{\sqrt{3}}{2} \\ \frac{\sqrt{3}}{2} & -\frac{1}{2} \end{pmatrix}$	$\begin{pmatrix} -1 & 0 \\ 0 & 1 \end{pmatrix}$	$\begin{pmatrix} \frac{1}{2} & \frac{\sqrt{3}}{2} \\ -\frac{\sqrt{3}}{2} & -\frac{1}{2} \end{pmatrix}$	1
E_2	$\begin{pmatrix} 1 & 0 \\ 0 & -1 \end{pmatrix}$	$\begin{pmatrix} -\frac{1}{2} & \frac{\sqrt{3}}{2} \\ \frac{\sqrt{3}}{2} & \frac{1}{2} \end{pmatrix}$	$\begin{pmatrix} -\frac{1}{2} & \frac{\sqrt{3}}{2} \\ \frac{\sqrt{3}}{2} & \frac{1}{2} \end{pmatrix}$	$\begin{pmatrix} -\frac{1}{2} & \frac{\sqrt{3}}{2} \\ \frac{\sqrt{3}}{2} & \frac{1}{2} \end{pmatrix}$	$\begin{pmatrix} 1 & 0 \\ 0 & -1 \end{pmatrix}$	$\begin{pmatrix} -\frac{1}{2} & \frac{\sqrt{3}}{2} \\ -\frac{\sqrt{3}}{2} & \frac{1}{2} \end{pmatrix}$	0

$$\begin{aligned}
H_{\chi}^{r_{\kappa',\kappa}}(\chi_j, \chi_i) &= \sum_R H_{\chi}(\chi_j, R\chi_i) \Gamma_{\kappa',\kappa}^{[z]*}(R) \\
&= \sum_R H_{\chi}(R\chi_i, \chi_j) \Gamma_{\kappa',\kappa}^{[z]*}(R) \\
&= \sum_R H_{\chi}(R^{-1}\chi_i, \chi_j) \Gamma_{\kappa',\kappa}^{[z]*}(R^{-1}) \\
&= \sum_R H_{\chi}(R^{-1}\chi_i, \chi_j) \Gamma_{\kappa',\kappa}^{[z]*-1}(R) \\
&= \sum_R H_{\chi}(R^{-1}\chi_i, \chi_j) \Gamma_{\kappa',\kappa}^{[z]*\dagger}(R) \\
&= \sum_R H_{\chi}(R^{-1}\chi_i, \chi_j) \Gamma_{\kappa,\kappa'}^{[z]}(R). \quad (\text{A4})
\end{aligned}$$

Because $H_{\chi}(\chi_i, \chi_j)$ ($DAF^{(2)}(\chi_i - \chi_j)$) depends on $|\chi_i - \chi_j|$, and R is a length-preserving operation, we have

$$\begin{aligned}
H_{\chi}(R^{-1}\chi_j, \chi_i) &= H_{\chi}(R^{-1}\chi_j, \chi_i) \\
&= H_{\chi}(RR^{-1}\chi_j, R\chi_i) = H_{\chi}(\chi_j, R\chi_i). \quad (\text{A5})
\end{aligned}$$

Combining Eq. (A4) and Eq. (A5) gives

$$H_{\chi_{\kappa,\kappa'}}^r(\chi_i, \chi_j) = \sum_R H_{\chi}(\chi_i, R\chi_j) \Gamma_{\kappa,\kappa'}^{[z]}(R). \quad (\text{A6})$$

Therefore, if $\Gamma^{[z]}$ is real, Eq. (A2) is true, and H_{χ}^r is symmetric.

APPENDIX B: IRREDUCIBLE REPRESENTATIONS OF GROUP C_2 , C_{2v} AND C_{6v}

The irreducible representation matrices for some point groups frequently used in APH surface function computations are given in Tables VII, VIII, and IX. The first column in each table gives the names of the irreducible representations. The second row gives the transformation when a symmetry operation R acts on χ . The parity p is also given in each table.

¹See *Advances in Molecular Vibrations and Collision Dynamics*, edited by J. M. Bowman (JAI, Greenwich, CT, 1994), Vols. 2A and 2B.

²*Dynamics of Molecules and Chemical Reactions*, edited by R. E. Wyatt and J. Z. H. Zhang (Dekker, New York, 1996).

³H. Nakamura, *Annu. Rev. Phys. Chem.* **48**, 299 (1997).

⁴G. Nyman and H. G. Wu, *Rep. Prog. Phys.* **63**, 1 (2000).

⁵L. D. Faddeev, *Mathematical Aspects of the Three-Body Problem in Quan-*

tum Scattering Theory (Israel Program for Scientific Translation, Jerusalem. Published in the USA by Davey, New York, 1965). For a review, see J. C. Y. Chen, *Case Stud. At. Phys.* **3**(5), 305 (1973).

⁶L. M. Delves, *Nucl. Phys.* **A9**, 391 (1959); **A20**, 275 (1960).

⁷B. D. Esry, C. H. Greene, and J. P. Burke, Jr., *Phys. Rev. Lett.* **83**, 1751 (1999).

⁸J. M. Launay and M. LeDourneuf, *Chem. Phys. Lett.* **169**, 473 (1990); J. M. Launay, *Theor. Chim. Acta* **79**, 183 (1991).

⁹R. T Pack and G. A. Parker, *J. Chem. Phys.* **87**, 3888 (1987).

¹⁰R. T Pack and G. A. Parker, *J. Chem. Phys.* **90**, 3511 (1989).

¹¹A. Kuppermann and P. G. Hipes, *J. Chem. Phys.* **84**, 5962 (1986); S. A. Cucaro, P. G. Hipes, and A. Kuppermann, *Chem. Phys. Lett.* **154**, 155 (1989); **157**, 440 (1989).

¹²Cf. U. Manthe, T. Seideman, and W. H. Miller, *J. Chem. Phys.* **99**, 10078 (1993); D. Neuhauser, *ibid.* **100**, 9272 (1994); D. H. Zhang and J. Z. H. Zhang, *ibid.* **101**, 1146 (1994); D. H. Zhang and J. C. Light, *ibid.* **105**, 1291 (1996); W. Zhu, J. Dai, J. Z. H. Zhang, and D. H. Zhang, *ibid.* **105**, 4881 (1996).

¹³B. Lepetit and J. M. Launay, *J. Chem. Phys.* **95**, 5159 (1991).

¹⁴Z. Bačić, J. D. Kress, G. A. Parker, and R. T Pack, *J. Chem. Phys.* **92**, 2344 (1990).

¹⁵J. D. Kress, Z. Bačić, G. A. Parker, and R. T Pack, *J. Phys. Chem.* **94**, 8055 (1990).

¹⁶J. M. Launay and M. LeDourneuf, *Chem. Phys. Lett.* **163**, 178 (1989).

¹⁷J. Linderberg, S. B. Padkjaer, Y. Ohrn, and B. Vessal, *J. Chem. Phys.* **90**, 6254 (1989).

¹⁸A. Laganà, R. T Pack, and G. A. Parker, *Faraday Discuss. Chem. Soc.* **84**, 409 (1987); **91**, 386 (1991).

¹⁹G. A. Parker, R. T Pack, A. Laganà, B. J. Archer, J. D. Kress, and Z. Bačić, in *Super Computer Algorithms for Reactivity, Dynamics and Kinetics of Small Molecules*, edited by A. Laganà (Kluwer, Dordrecht, 1989), p. 105.

²⁰J. D. Kress, Z. Bačić, G. A. Parker, and R. T Pack, *Chem. Phys. Lett.* **157**, 484 (1989).

²¹J. D. Kress, R. T Pack, and G. A. Parker, *Chem. Phys. Lett.* **170**, 306 (1990).

²²J. D. Kress, *Chem. Phys. Lett.* **179**, 510 (1991).

²³L. Wolniewicz, *J. Chem. Phys.* **90**, 371 (1989).

²⁴G. A. Parker and R. T Pack *J. Chem. Phys.* **98**, 6883 (1993).

²⁵S. S. Iyengar, G. A. Parker, D. J. Kouri, and D. K. Hoffman, *J. Chem. Phys.* **110**, 10283 (1999).

²⁶D. K. Hoffman, T. L. Marchioro, II, M. Arnold, Y. Huang, W. Zhu, and D. J. Kouri, *J. Math. Chem.* **20**, 117 (1996).

²⁷See Ref. 14 and references therein.

²⁸J. Z. H. Zhang, *Chem. Phys. Lett.* **181**, 63 (1991).

²⁹F. B. Brown, R. Steckler, D. W. Schwenke, D. G. Truhlar, and B. C. Garrett, *J. Chem. Phys.* **82**, 188 (1985); R. Steckler, D. G. Truhlar, and B. C. Garrett, *ibid.* **82**, 5499 (1985).

³⁰M. Weissbluth, *Atoms and Molecules* (Academic, London, 1978).

³¹C. H. Yu, D. J. Kouri, M. Zhao, D. G. Truhlar, and D. W. Schwenke, *Chem. Phys. Lett.* **157**, 491 (1989); *Int. J. Quantum Chem., Quantum Chem. Symp.* **23**, 45 (1989).

³²D. E. Manolopoulos, M. D'Mello, and R. E. Wyatt, *J. Chem. Phys.* **93**, 403 (1990).

³³D. Neuhauser, M. Baer, R. S. Judson, and D. J. Kouri, *Chem. Phys. Lett.* **169**, 372 (1990); D. Neuhauser, R. S. Judson, R. L. Jaffe, M. Baer, and D. J. Kouri, *ibid.* **176**, 546 (1991).

³⁴D. T. Colbert and W. H. Miller, *J. Chem. Phys.* **96**, 1982 (1991).